

Radio interferometric observations of candidate water-maser-emitting planetary nebulae

José F. Gómez¹, Olga Suárez², Yolanda Gómez³, Luis F. Miranda¹, José M. Torrelles⁴,
Guillem Anglada¹, Óscar Morata⁵

ABSTRACT

We present Very Large Array (VLA) observations of H₂O and OH masers, as well as radio continuum emission at 1.3 and 18 cm toward three sources previously cataloged as planetary nebulae (PNe) and in which single-dish detections of H₂O masers have been reported: IRAS 17443–2949, IRAS 17580–3111, and IRAS 18061–2505. Our goal was to unambiguously confirm their nature as water-maser-emitting PNe, a class of objects of which only two bona-fide members were previously known. We detected and mapped H₂O maser emission toward all three sources, while OH maser emission is detected in IRAS 17443–2949 and IRAS 17580–3111 as well as in other two objects within the observed fields: IRAS 17442–2942 (unknown nature) and IRAS 17579–3121 (also cataloged as a possible PN). We found radio continuum emission associated only with IRAS 18061–2505. Our results confirm IRAS 18061–2505 as the third known case of a PN associated with H₂O maser emission. The three known water-maser-emitting PNe have clear bipolar morphologies, which suggests that water maser emission in these objects is related to non-spherical mass-loss episodes. We speculate that these bipolar water-maser-emitting PNe would have “water-fountain” Asymptotic Giant Branch (AGB) and post-AGB stars as their precursors. A note of caution is given for other objects that have been classified as OHPNe (objects

¹Instituto de Astrofísica de Andalucía, CSIC, Apartado 3004, E-18080 Granada, Spain; e-mail: jfg@iaa.es; lfm@iaa.es; guillem@iaa.es

²Laboratoire Hippolyte Fizeau, Université de Nice, Parc Valrose, 06108 Nice cedex 02, France; e-mail: olga.suarez@unice.fr

³Centro de Radioastronomía y Astrofísica, UNAM, Campus Morelia, Apdo. Postal 3-72, Morelia, Michoacán 58089, Mexico; e-mail: y.gomez@astrosmo.unam.mx

⁴Instituto de Ciencias de Espacio (CSIC)-IEEC, Facultat de Física, Planta 7a, Universitat de Barcelona, Martí i Franques, 08028 Barcelona, Spain; e-mail: torrelles@ieec.frc.es

⁵Laboratorio de Astrofísica Espacial y Física Fundamental, INTA, Apartado 50727, E-28080 Madrid, Spain

with both OH maser and radio continuum emission, that could be extremely young PNe) based on single-dish observations, since interferometric data of both OH masers and continuum are necessary for a proper identification as members of this class.

Subject headings: stars: AGB and post-AGB – planetary nebulae: general – planetary nebulae: individual (IRAS 18061–2505) – masers

1. Introduction

Maser emission from different molecules is found in the energetic environments of several types of astronomical objects, such as evolved stars, young stellar objects, or active galactic nuclei (Elitzur 1992). Masers have proven to be a very powerful tool to study the morphology and kinematics of the gas in these environments, since their high surface brightness makes them excellent targets for radio interferometric observations, including the use of Very Long Baseline Interferometry with angular resolutions under 1 milliarcsecond (e.g., Torrelles et al. 2002; Boboltz 2005). Therefore, they allow to study the inner few AU in young stellar objects and evolved stars, or 1 pc around active galactic nuclei.

Maser emission from SiO, OH, and H₂O are common in the circumstellar envelopes of oxygen-rich evolved stars. In the particular case of water masers, it was thought for some time that they disappear soon after (≤ 100 years) the Asymptotic Giant Branch (AGB) mass-loss stops, so they were not expected to be associated with PNe (Lewis 1989; Gómez et al. 1990). However, Miranda et al. (2001) reported the source K3-35 as the first confirmed case of a PN associated with water maser emission (hereafter H₂O-PN). Later, during a search for this type of masers toward 26 additional PNe, a new detection was found toward IRAS 17347–3139 (de Gregorio-Monsalvo et al. 2004). In these two cases, the association of the maser emission with the radio continuum emission from the ionized PN was confirmed via high-resolution interferometric observations using the Very Large Array (VLA).

Recently, Suárez, Gómez, & Morata (2007) carried out a single-dish survey for water masers in post-AGB stars and PNe selected by their IRAS colors in the atlas of Suárez et al. (2006). In that survey, water maser emission was found toward three objects previously cataloged as PNe (Ratag et al. 1990; Suárez et al. 2006): IRAS 17443–2949, IRAS 17580–3111, and IRAS 18061–2505. However, given the relatively large angular separation between the reported peak position of the radio continuum emission (Ratag et al. 1990) and the infrared sources in the region, Suárez et al. (2007) suggested that IRAS 17580–3111 is probably not a PN.

In this paper we present VLA observations of maser emission of H_2O and OH molecules, as well as radio continuum emission, toward IRAS 17443–2949, IRAS 17580–3111, and IRAS 18061–2505. Our main goal was to confirm the association of the water maser emission with these candidates to PNe. It is also interesting to check whether these masers are pumped within a few tenths of AU from the central star, as seen in IRAS 17347–3139 (de Gregorio-Monsalvo et al. 2004) and the inner region of K3-35 (Miranda et al. 2001), or they can also be pumped in shocked outer regions of the PN lobes, as in K3-35 (Miranda et al. 2001). With the evidence provided in this paper, we can ascertain that IRAS 18061–2505 is the third confirmed case of an H_2O -PN.

2. Observations

We observed two OH maser transitions at $\simeq 1.6 - 1.7$ GHz and the $6_{16} - 5_{23}$ transition of the water molecule at $\simeq 22$ GHz, as well as radio continuum emission at both $\simeq 1.7$ and 22 GHz, toward IRAS 17443–2949, IRAS 17580–3111, and IRAS 18061–2505, using the VLA of the National Radio Astronomy Observatory (NRAO)¹. The details of the observations are listed in Tables 1, 2, and 3. In all cases, both right and left circular polarization were observed. We note that a continuum dataset at 1.7 GHz, with a bandwidth of 25 MHz, was obtained simultaneously with the OH line at 1665 MHz. However, these continuum data were not usable due to radio frequency interference. An alternative continuum dataset at that frequency was obtained by averaging line-free channels in the OH spectral data at 1665 MHz. The H_2O maser and radio continuum observations at $\simeq 22$ GHz were also carried out simultaneously.

The data were calibrated and processed using the Astronomical Image Processing System (AIPS) of the NRAO. Maps were obtained with robust weighting (robust parameter = 0) of visibilities (Briggs 1995), using the AIPS task IMAGR. When a maser line was detected, self-calibration was applied on the channel with maximum emission. The self-calibration solutions were then applied to all channels and, in the case of the H_2O masers, these solutions were also applied to the simultaneous radio continuum observations at 22 GHz. For the OH data at 1665 MHz in IRAS 17443–2949, self-calibration was applied to the continuum emission from GAL 359.23–00.82 (The Mouse Nebula, detected by Yusef-Zadeh & Bally 1987), which fell within the primary beam; this continuum emission was extracted by integrating 116 channels from the dataset. When present, continuum emission was subtracted from

¹ The National Radio Astronomy Observatory is a facility of the National Science Foundation operated under cooperative agreement by Associated Universities, Inc.

line data using the AIPS task UVLIN. Some line data sets had to be Hanning-smoothed in frequency (see Table 4), to alleviate spectral ripples due to the Gibbs phenomenon.

3. Results

3.1. Detected emission

Our results are summarized in Tables 4 and 5. We have detected and mapped H₂O maser emission toward all three target sources. OH maser emission at 1612 MHz was detected in IRAS 17443–2949 and IRAS 17580–3111, but not in IRAS 18061–2505. OH emission at 1665 MHz was only detected in IRAS 17443–2949. As for the radio continuum emission, it was only detected associated with IRAS 18061–2505, at both 1.7 and 22 GHz .

In addition to this, OH maser emission at 1612 MHz was detected toward two additional sources that lie within the field of view of the observations (primary beam $\simeq 28'$): IRAS 17442–2942 (within the primary beam of the observations toward IRAS 17443–2949), and IRAS 17579–3121 (within the primary beam from IRAS 17580–3111). These additional two sources were well outside the corresponding primary beam of the 22 GHz observations ($\simeq 2'$ size), so it is not possible to know whether they are associated with H₂O maser emission.

In the following sections we present the spectra and maps of the maser emission toward all five sources.

3.2. Individual objects: target sources

3.2.1. IRAS 17443–2949

This source has been classified as PN, based on the detection of radio continuum emission (Ratag et al. 1990), with a flux density $S_\nu(6\text{cm}) \simeq 0.9$ mJy. Water maser spectra obtained by Suárez et al. (2007) showed two well-defined spectral components separated by 2 km s^{-1} , centered at $\simeq -5 \text{ km s}^{-1}$. Maser emission of OH at 1612 MHz was previously reported by Zijlstra et al. (1989), with a single peak at $\sim -15 \text{ km s}^{-1}$. These authors also point out that OH emission coincides, within the errors, with the radio continuum emission.

Our H₂O maser spectrum shows four spectral components above the noise level (Table 4 and Fig. 1), although the component at -1.7 km s^{-1} is significantly weaker than the other three and it is difficult to distinguish in Fig. 1. The two most intense components correspond to the ones detected in the single-dish observations of Suárez et al. (2007). The H₂O maser

components are closely clustered in space (Table 4), within a region of $\simeq 80$ milliarcsec. No obvious spatio-kinematical distribution is seen, and therefore it is not possible to determine what kind of structure the water masers are tracing.

We have detected both OH lines at 1612 and 1665 MHz in this object (for the first time in the case of the latter transition). The spectrum of the 1612-MHz line shows a double peak, although very asymmetric, with the component at $V_{\text{LSR}} \simeq -16.1 \text{ km s}^{-1}$ being ~ 20 times stronger than the one at $\simeq -4.8 \text{ km s}^{-1}$ (Fig. 1). The OH spectrum at 1665 MHz shows also a peak close in velocity to that at 1612 MHz, with at least three additional spectral features covering the velocity range in which H_2O masers are also detected. The two components of the OH 1612-MHz spectrum appear significantly separated in space ($\simeq 3''$). The H_2O masers lie midway between these two OH 1612-MHz components (Fig. 2). On the other hand, given the large relative positional errors for the OH 1665 MHz emission, it is not possible to determine its real spatial distribution.

Fig. 2 shows the possible infrared counterparts for the object powering the masers. We have checked both the MSX (Egan et al. 2003) and 2MASS (Skrutskie et al. 2006) catalogs, in the mid- and near-infrared ranges, respectively, to search for a counterpart of the IRAS source that could be the exciting source of the maser emission. The infrared point source that is closer to the maser positions is MSX6C G359.4428-00.8398, which also lies within the error ellipse of IRAS 17443–2949. Its position is consistent, within the errors, with the OH 1665-MHz emission and one of the OH 1612-MHz components.

We did not detect radio continuum emission, either at 1.7 or 22 GHz (Table 5), that could be associated with the maser emission. The radio continuum source at 4.9 GHz reported by Ratag et al. (1990) is $\simeq 9''$ away from the position of the water masers and $10''$ from the MSX source. We note that the beam of the Ratag et al. (1990) observations was $\simeq 5'' - 10''$, although we would expect their absolute positional accuracy to be somewhat better than that. We think it is unlikely that the masers (specially those of H_2O , with a better absolute positional accuracy, $\simeq 0''.2$) are associated with the reported radio continuum emission. Therefore, we do not have enough evidence to support that the maser emission we detected may be pumped by a PN.

The identification of IRAS 17443–2949 itself as a PN is also questionable. Recently, García-Hernández et al. (2007) suggested that this source is still in the AGB phase, given its high variability in the infrared and the presence of strong amorphous silicate absorption features in its infrared spectrum. Its AGB status, together with the presence of OH and H_2O emission, and its unlikely association with radio continuum emission, lead us to classify this source as an OH/IR star, rather than pertaining to the OHPN class defined by Zijlstra et al. (1989).

3.2.2. IRAS 17580–3111

This source has also been classified as a PN, with detected radio continuum emission at a level of $S_\nu(6\text{cm}) \simeq 2.5$ mJy (Ratag et al. 1990). Suárez et al. (2007) detected water maser emission, dominated by a component at ~ 21 km s⁻¹. OH maser emission at 1612 MHz was detected by Zijlstra et al. (1989), showing at least four spectral components. These authors pointed out the need of VLA observations to determine whether more than one source within the beam of their observations could be contributing to the OH spectrum.

Our H₂O maser data shows only one component (Fig. 3), at 17.4 km s⁻¹. The OH 1612-MHz spectrum shows a typical two-peaked spectrum (Fig. 3), whose components coincide in velocity with two of the four components detected by Zijlstra et al. (1989). The remaining two components seen by these authors may be associated with the source IRAS 17579–3131 (see sec. 3.3.2), located $\simeq 11'$ away from IRAS 17580–3111, although the former is outside the half-power beam of the telescope ($\simeq 12'.6$) in their single-dish observations. The positions of the two OH components we detected are consistent with each other, within their relative errors (Table 4). No OH maser at 1665 MHz, nor radio continuum emission at either 1.7 or 22 GHz was detected (Tables 4, 5).

Fig. 4 shows the position of all maser components and infrared point sources in their neighborhood. There is a mid-infrared source (MSX6C G359.7798-04.0728) and a near infrared one (2MASS J18012040-3111203) close to the masers. Both infrared sources as well as the H₂O and OH maser components lie within the error ellipse of IRAS 17580–3111. The IRAS, MSX, and 2MASS fluxes are, in principle, compatible with belonging to the same object. However, the error ellipses quoted in the MSX and 2MASS catalogs do not intersect, so they might actually be tracing different sources. Given its position, the object 2MASS J18012040-3111203 is the most likely candidate to be the powering source of the maser emission.

Regarding the nature of the object, as already pointed out by Suárez et al. (2007), the radio continuum source reported by Ratag et al. (1990) is more than 30'' away from the infrared sources and the maser emission of both OH and H₂O, and therefore, it is not associated with them. The identification of IRAS 17580–3111 as a PN on the basis of the presence of radio continuum emission is not well justified. García-Hernández et al. (2007) also presented infrared spectroscopy toward this IRAS source; its spectrum and its low variability in the infrared led these authors to classify IRAS 17580–3111 as a post-AGB star.

3.2.3. IRAS 18061–2505

This source was first cataloged as a PN by MacConnell (1978) (object Mac 1-10). It shows a bipolar morphology with two well-defined lobes seen in the H_α image (Suárez et al. 2006), with a total size of $\simeq 46''$. Images of the continuum close in wavelength to the H_α line, as well as two-dimensional spectroscopy (Suárez et al. 2008, in preparation) clearly show that the lobes are ionized. This source also shows radio continuum emission at 1.4 GHz in the NRAO/VLA Sky Survey (Condon & Kaplan 1998), with a flux density of 3.5 ± 1.0 mJy, at R.A.(J2000) = $18^h09^m12^s.9$, Dec(J2000) = $-25^\circ04'27''$ (positional error $\simeq 7''$). Suárez et al. (2007) detected water maser emission, with three highly-variable components.

We detected water maser emission toward IRAS 18061–2505 (Fig. 5). No OH maser emission at either 1612 or 1665 MHz was detected. The H_2O maser emission exhibits three distinct spectral features, at $\simeq 57$, 61, and 64 km s^{-1} . We also detected unresolved radio continuum emission at 1.7 and 22 GHz from the ionized region associated with this source (Table 5), whose position is consistent with that given by Suárez et al. (2006) for the central region of the cataloged PN. We did not detect continuum emission in the large ionized lobes seen in the H_α image. The dynamic range of our radio continuum map at 22 GHz is $\simeq 400$ (rms $\simeq 90 \mu\text{Jy beam}^{-1}$), and the emission from the extended lobes must be below the sensitivity level imposed by this dynamic range. The positions of the infrared sources 2MASS J18091242-2504344 and MSX6C G005.9737-02.6115 are consistent, within the errors, with the position of the radio continuum source.

The nominal positions of these maser features are all within 50 mas (65 AU assuming a distance of 1.3 kpc, Preite-Martinez 1988) from one another and from the radio continuum emission, which confirms that IRAS 18061–2505 is the third PN known to harbor water masers. We note that no water maser emission has been found associated with the extended lobes of the PN. It still remains to be determined whether the water maser emission found associated with the central source could be tracing the inner part of a jet or a circumstellar structure, such as a disk or torus. However, the latter possibility seems likely, given that water masers in the other two known H_2O -PNe (Miranda et al. 2001; de Gregorio-Monsalvo et al. 2004; Uscanga et al. 2008, in preparation) seem to preferentially trace toroidal structures. A confirmation of the spatial distribution of water masers in IRAS 18061–2505 would only be possible with a more extended VLA configuration or with VLBI networks.

Using our radio continuum data, we can make a rough estimate of the spectral index of $\alpha = 0.92 \pm 0.13$ ($S_\nu \propto \nu^\alpha$) between 1.4 and 22 GHz. This index is similar to the one found in IRAS 17347–3139, $\alpha = 0.79 \pm 0.04$, between 4.3 and 8.9 GHz (Gómez et al. 2005a), whose rising spectral energy distribution beyond 10 GHz was suggested to be a signature of youth. Simultaneous observations of radio continuum at different frequencies would be

necessary to obtain a proper estimate of the spectral index and the turnover frequency of IRAS 18061–2505, to derive physical properties such as its emission measure and electron density.

We also note that, among the three confirmed PNe with water masers, this is the only one with no detectable OH maser emission, and it is also the one with the largest angular size (cf: Miranda et al. 2001; de Gregorio-Monsalvo et al. 2004; Suárez et al. 2006).

3.3. Individual objects: other sources in the fields

3.3.1. IRAS 17442–2942

This source is cited in the SIMBAD database as associated to the gamma-ray source 3EG J1744-3011 in the third EGRET catalog (Hartman et al. 1999), or 2EG J1747-3039 in their second catalog (Thompson et al. 1995). However, the IRAS position is 1.3 and 0.7 degrees, away from the positions in the third and second EGRET catalogs, respectively. This means that the IRAS source is outside the error ellipse of the gamma-ray source (0.32 and 0.2 degrees, depending on the catalog version). Therefore, we think that the identification of the IRAS source with the gamma-ray source is incorrect.

We have detected OH 1612-MHz emission associated with IRAS 17442–2942 (Fig. 7 and Table 4), which was within the primary beam of our observation toward IRAS 17443–2949. There are two well-defined velocity components, separated by $\simeq 30 \text{ km s}^{-1}$. No OH maser at 1665 MHz nor radio continuum emission at 18 cm has been detected. This source is well outside the primary beam of the H₂O observations, so it is not possible to determine whether there is any H₂O maser emission associated with this object.

Both OH components are located midway between two infrared sources of the 2MASS catalog, 2MASS J17472879-2943392 and 2MASS 17472898-2943369 (Fig. 8), but it is not possible to determine whether either of them is pumping the maser. With the scarce information available, we do not know the evolutionary stage of the pumping source of the maser emission in this region.

3.3.2. IRAS 17579–3121

This source is also listed as a PN by Ratag et al. (1990), although it shows an optical spectrum typical of a post-AGB star (Suárez et al. 2006). The radio continuum source reported by Ratag et al. (1990) has a flux density $S_\nu(6\text{cm}) \simeq 0.8 \text{ mJy}$ and is $\simeq 12''$ from

the possible infrared counterparts of this evolved object (2MASS J18011337-3121566 and MSX6C G359.6129-04.1379), although all these sources are within the error ellipse of IRAS 17579–3121. Slysh et al. (1997) reported a single-dish detection of OH maser emission at 1667 MHz, although it may actually arise from IRAS 17580–3111, since the position of this source is close to the half-power level of the telescope beam in their observations.

This source was within the primary beam of our OH observations toward IRAS 17580–3111. We detected OH maser emission at 1612 MHz, but not at 1665 MHz. It shows three distinct spectral components (Fig. 9 and Table 4). The two strongest components may account for two of the four ones detected in the single-dish observations of IRAS 17580–3111 reported by Zijlstra et al. (1989). All three OH components are coincident, within the errors, with 2MASS J18011337-3121566. No radio continuum emission at 18 cm has been detected. The source is also well outside the primary beam of the H₂O observations and therefore, it is not possible to determine its association with H₂O maser emission.

4. Discussion

4.1. H₂O and OH masers and the evolution of bipolar PNe

One of the main results in this paper is the confirmation of IRAS 18061–2505 as a water-maser-emitting PN. This is the third object that could be considered a bona fide H₂O-PN, only after K3-35 (Miranda et al. 2001) and IRAS 17347–3139 (de Gregorio-Monsalvo et al. 2004). In classical studies of maser emission in evolved stars, water masers were not expected in stages as late as PNe. However, since the number of known cases is growing, it seems interesting to review the characteristics of H₂O-PNe, and how they fit in the general scheme of late stellar evolution.

Many previous studies of maser emission (of SiO, H₂O, and OH molecules) in evolved stars focused on the AGB phase, mainly Mira-type and OH/IR stars. OH maser emission in these objects (and in a significant fraction of post-AGB stars) typically shows double-peaked profiles, specially for the 1612 MHz transition, with narrow components separated by $\lesssim 30 \text{ km s}^{-1}$ (e.g., Eder et al. 1988; Sevenster et al. 1997). These profiles have been interpreted as arising from the approaching and receding sides of an spherically-symmetric, expanding envelope (Reid et al. 1977). This seems to be the case of IRAS 17580–3111 or IRAS 17442–2942 (Figs. 3 and 7) in this paper. In some cases only one peak is detected, which could be due to sensitivity limitations if the spectrum is asymmetric, with one of the peaks significantly weaker than the other. Emission of H₂O and SiO tend also to be double- or single-peaked, with their spectral components encompassed within the range marked by

the two peaks of the OH emission at 1612 MHz. The presence of different maser transitions was used by Lewis (1989) to construct a chronological sequence, in which masers appear and disappear sequentially as the star evolves from the AGB to the PN phase. However, as noted by Lewis (1989), this chronological sequence is only valid for the case of spherically symmetrical mass-loss, and it will not stand if bipolar mass loss is present.

The presence of maser spectra not following the regular double (or single) peak pattern, or with H₂O maser emission extending outside the velocity range covered by OH emission, are interpreted as evidence of non-spherical mass-loss processes (e.g., Gómez et al. 1994; Deacon et al. 2004). That would be the case of sources IRAS 17443–2949, IRAS 18061–2505, or IRAS 17579–3121 (Figs. 1, 5, and 9) in this paper. A significant fraction of OH and H₂O maser spectra in post-AGB stars do show multiple velocity components (Sevenster 2002; Engels 2002). Specially significant is the case of “water fountain” sources (Likkell & Morris 1988; see Imai 2007 for a review). These are late-AGB and post-AGB stars which show H₂O maser components spanning $\gtrsim 100 \text{ km s}^{-1}$, i.e., significantly larger than the few tens of km s^{-1} that characterize the spherical wind in the AGB. Water emission in water fountain sources traces highly collimated and symmetrical jets, with dynamical ages of 10-100 yr (Sahai et al. 1999; Imai et al. 2002; Claussen et al. 2004; Imai et al. 2007; Imai 2007; Morris et al. 2003; Boboltz & Marvel 2007). These sources represent the earliest known manifestation of non-spherical mass-loss in evolved stars. We also note that, in some of these sources, in addition to the high-velocity maser components associated with the jet, there are low-velocity components located close to the dynamical center of the jet (Imai 2007). These components could trace low-velocity equatorial flows, or expanding toroidal structures.

Focusing again on H₂O-PNe, a key common property is that all three confirmed cases show a clear bipolar morphology at optical, infrared, and/or radio continuum (Miranda et al. 2001; de Gregorio-Monsalvo et al. 2004; Suárez et al. 2006). This could indicate that water masers in PNe are related to non-spherical mass-loss phenomena, rather than being the remnant of the masers excited in the (spherical) AGB wind (Suárez et al. 2007). As discussed elsewhere (e.g. Engels 2002; Deacon et al. 2007; Suárez et al. 2007), the presence of water fountains and H₂O-PNe shows that H₂O masers in evolved stars could be pumped in two different phases: by spherical winds during the AGB phase, and later, by highly collimated winds that turn on close to the end of the AGB phase for a particular type of stars (probably the most massive precursors of PNe). The sources in which H₂O masers are excited by these collimated jets would first appear as water fountains and, following Suárez et al. (2007), we speculate that some of them might evolve to become H₂O-PNe.

We note here the different distributions and kinematics of H₂O maser emission in wa-

ter fountains and H₂O-PNe. While H₂O maser emission in water fountains always traces high-velocity bipolar jets, with additional low-velocity equatorial structures in some cases (Imai 2007), the emission in H₂O-PNe tends to trace compact, low-velocity equatorial structures. Only in one epoch, in the H₂O-PN K3-35, water maser emission was detected associated with a bipolar jet (Miranda et al. 2001), although with a much lower line-of-sight velocity ($\leq 5 \text{ km s}^{-1}$) than jets traced by masers in water fountains. Water masers tracing jets have not been seen in subsequent observations of K3-35, neither in IRAS 17347–3139 (de Gregorio-Monsalvo et al. 2004), which suggests that this could be a transient phenomenon in H₂O-PNe.

To explain the short dynamical ages of water fountains ($\lesssim 100 \text{ yr}$), Imai et al. (2007) suggested that the high-velocity, collimated jet drills through the circumstellar envelope previously expelled during the AGB phase. Shocks between the jet and the envelope excite H₂O masers along the jet direction. A possible coeval equatorial flow could excite water masers along a perpendicular direction. When the jet reaches the lower density regions in the outer envelope, water masers can no longer be pumped along the jet. A jet of $\simeq 100 \text{ km s}^{-1}$ would advance $\simeq 2000 \text{ AU}$ in $\simeq 100 \text{ yr}$, which is the typical size for circumstellar envelopes in OH/IR stars. At that point, these sources would stop showing the characteristic maser emission of water fountains, although jets could still be active, even during the PN phase (Velázquez et al. 2007).

If we extrapolate this scenario beyond the point at which the high-velocity masers of the water-fountain jets turn off, the equatorial regions are the only ones close enough to the central star and with the necessary high density to eventually support water maser emission. By the time the central source starts the ionization of its envelope, masers could be excited preferentially in equatorial regions (circumstellar disks or equatorial flows), as seen in H₂O-PNe. Dense molecular gas has been found in K3-35 (Tafoya et al. 2007), providing the conditions in which molecules like H₂O can survive in the ionizing environment of a PN (Tafoya et al. 2007).

Summarizing, we propose the following scenario for water maser emission during the evolution toward bipolar PNe:

1. Water-fountain phase. Water masers preferentially trace a high-velocity jet and, in some cases, equatorial regions. This phase ends when the jet reaches regions with a density too low for water masers to be excited.
2. H₂O-PN phase. Young bipolar PNe, with its ionized structure extending along the lower-density bipolar cavity previously opened by jets. Water masers could be excited mostly in the denser equatorial regions.

Whether there is a significant gap between these two phases, or they overlap, would probably depend on the mass of the progenitor star. However, since the progenitors of bipolar PNe are thought to be relatively massive, their evolution would be fast, and ionization could start soon after the onset of bipolar mass-loss. In this case, the two phases mentioned above could overlap, and at some point of their evolution they could be PNe with water-fountain characteristics. No water-fountain PN has been confirmed so far, but if any such object exists, our evolutionary scenario would indicate that it should have a high optical extinction (thus making difficult its identification as a PN) and the mass of its progenitor star should be in the upper ranges for PNe ($\simeq 8 M_{\odot}$).

We note that, in our scenario, not all water fountains may necessarily end up as H₂O-PNe, if the circumstellar envelope has been significantly cleared, even in equatorial regions, so that the conditions to pump water masers are not met anywhere in the circumstellar envelope by the time ionization starts. However, we think it likely that all H₂O-PNe have gone through a phase with collimated jets, probably shown as water fountains.

4.2. A note on planetary nebulae with OH emission (OHPNe)

The apparent non-association of water masers with radio continuum emission in IRAS 17443–2949 and IRAS 17580–3111 is also worth noting. Both sources have been previously classified as PNe on the basis of presence of radio continuum emission (Ratag et al. 1990). The detection of OH emission made Zijlstra et al. (1989) to include them in a special class of objects, OHPNe. This type of objects, showing both OH and radio continuum emission, and strongly obscured or invisible in the optical, were suggested to form an evolutionary phase immediately before the formation of a full-blown PN. Therefore, they are potentially key objects to study the early evolution of PNe, including the processes that may give rise to the different morphologies observed in these nebulae.

Our results, using an angular resolution higher than that available in the data presented by Zijlstra et al. (1989), suggest that in IRAS 17443–2949 and IRAS 17580–3111, OH and H₂O maser emission is not associated with the reported radio continuum emission and, therefore, they are not proper members of the OHPN class. We also note that Ratag et al. (1990) reported radio continuum emission toward IRAS 17579–3121, and we have detected OH maser emission, although its angular separation to the radio continuum is too large to be associated, and thus, this source should not be considered an OHPN either.

Therefore, it seems very important to carry high angular and spectral resolution studies of maser and radio continuum emission in all sources that have been proposed as candidates

to being OHPNe, before drawing any further conclusions about their properties as a group and their relevance as a link between the post-AGB and PN phase. For some objects, such as K3-35 and IRAS 17347–3139, observations with high enough angular resolution allow us to include them as proper members of the OHPN class. Other prospective OHPNe would probably need more detailed research before being unambiguously included within this class of objects.

5. Conclusions

We have presented VLA observations of OH (1612 and 1665 MHz) and water masers (22235 MHz) as well as radio continuum emission at 1.3 and 18 cm toward three possible water-maser-emitting PN: IRAS 17443–2949, IRAS 17560–3111, and IRAS 18061–2505. Our main conclusions are as follow:

- We have detected water maser emission toward all target sources. OH maser emission at 1612 MHz is found associated with IRAS 17443–2949 and IRAS 17560–3111, as well as toward two other objects within the observed fields: IRAS 17442–2942 (unknown nature) and IRAS 17579–3121 (previously cataloged as a possible PN). OH maser emission at 1665 MHz is present in IRAS 17443–2949. Radio continuum emission at 1.3 and 18 cm was detected only toward IRAS 18061–2505.
- The water maser and radio continuum emission in IRAS 18061–2505 is found within a region of 50 mas in size, coincident with the central region of the large ($\simeq 46''$ size) PN seen in the optical images. This confirms this object as the third known water-maser-emitting PN. The three confirmed H₂O-PNe have clear bipolar morphologies, which suggest that the water maser emission in these objects is not the remnant of the maser emission pumped by spherical winds in the AGB phase.
- For the other objects previously cataloged as possible PNe (IRAS 17443–2949, IRAS 17560–3111, and IRAS 17579–3121), the positions of the OH and/or H₂O maser emission and those of the most likely near- and mid-infrared counterparts of the IRAS sources are not consistent with the positions of the radio continuum emission reported in the literature. Therefore, these IRAS sources are not likely to trace PNe.
- We suggest an evolutionary scheme in which the precursors of H₂O-PNe would be “water-fountain” AGB or post-AGB stars. Water maser emission in these fountains tend to trace highly collimated jets (and equatorial structures in some cases). The jet clears the circumstellar envelope along the polar direction and, therefore, water masers in PNe are found preferentially tracing equatorial structures.

- Although IRAS 17443–2949, IRAS 17560–3111, and IRAS 17579–3121 would be classified as OHPNe (objects with both OH maser and radio continuum emission, which have been suggested to be extremely young PNe) based on single-dish observations, our interferometric data indicate that they are not proper members of this class. Other prospective members of the OHPNe class will also need to be confirmed with interferometric observations, before drawing further conclusions about the properties of this class of objects.

JFG, JMT, GA, and OM acknowledge support from MEC (Spain) grant AYA 2005-08523-C03. LFM is supported by MEC grant AYA2005-01495. OS is partially supported by MEC grant AYA2003-09499. JFG, OS, LFM, JMT, and GA are also supported by Consejería de Innovación, Ciencia y Empresa of Junta de Andalucía. YG is supported by DGAPA-UNAM grant IN100407 and CONACyT grant 49947. This publication makes use of data products from the Two Micron All Sky Survey, which is a joint project of the University of Massachusetts and the Infrared Processing and Analysis Center/California Institute of Technology, funded by the National Aeronautics and Space Administration and the National Science Foundation.

REFERENCES

- Boboltz, D. A. 2005, in ASP Conf. Ser. 340, Future Directions in High Resolution Astronomy, ed. J. Romney & M. Reid (San Francisco: ASP), 342
- Boboltz, D. A., & Marvel, K. B. 2007, ApJ, 665, 680
- Briggs, D. S. 1995, PhD Thesis, New Mexico Institute of Mining and Technology
- Claussen, M., Sahai, R., & Morris, M. 2004, in ASP Conf. Proc. 313, Asymmetrical Planetary Nebulae III: Winds, Structure and the Thunderbird, ed. M. Meixner, J. H. Kastner, B. Balick, & N. Soker (San Francisco: ASP), 331
- Condon, J. J., & Kaplan, D. L. 1998, ApJS, 117, 361
- Deacon, R. M., Chapman, J. M., & Green, A. J. 2004, ApJS, 155, 595
- Deacon, R. M., Chapman, J. M., Green, A. J., & Sevenster, M. N. 2007, ApJ, 658, 1096
- de Gregorio-Monsalvo, I., Gómez, Y., Anglada, G., Cesaroni, R., Miranda, L. F., Gómez, J. F., & Torrelles, J. M. 2004, ApJ, 601, 921
- Eder, J., Lewis, B. M., & Terzian, Y. 1988, ApJS, 66, 183
- Egan, M. P., et al. 2003, VizieR Online Data Catalog, 5114, 0
- Elitzur, M. 1992, ARA&A, 30, 75.
- Engels, D. 2002, A&A, 388, 252
- García-Hernández, D. A., Perea-Calderón, J. V., Bobrowsky, M., & García-Lario, P. 2007, ApJ, in press
- Gómez, J. F., de Gregorio-Monsalvo, I., Lovell, J. E. J., Anglada, G., Miranda, L. F., Suárez, O., Torrelles, J. M., & Gómez, Y. 2005, MNRAS, 364, 738
- Gómez, Y., Moran, J. M., & Rodríguez, L. F. 1990, Rev. Mex. A&A, 20, 55
- Gómez, Y., Rodríguez, L. F., Contreras, M. E., & Moran, J. M. 1994, Rev. Mex. A&A, 28, 97
- Gómez, Y., Tafoya, D., Anglada, G., Franco-Hernández, R., Torrelles, J. M., & Miranda, L. F. 2005, Memorie della Societa Astronomica Italiana, 76, 472
- Hartman, R. C., et al. 1999, ApJS, 123, 79

- Imai, H. 2007, in IAU Symp. 242, *Astrophysical Masers and their Environments*, ed. W. Baan & J. Chapman (Cambridge: Cambridge Univ. Press), 279
- Imai, H., Obara, K., Diamond, P. J., Omodaka, T., & Sasao, T. 2002, *Nature*, 417, 829
- Imai, H., Sahai, R., & Morris, M. 2007, *ApJ*, 669, 424
- Lewis, B. M. 1989, *ApJ*, 338, 234.
- Likkell, L., & Morris, M. 1988, *ApJ*, 329, 914
- MacConnell, D. J. 1978, *A&AS*, 33, 219
- Miranda, L. F., Gómez, Y., Anglada, G., & Torrelles, J. M. 2001, *Nature*, 414, 284
- Morris, M. R., Sahai, R., & Claussen, M. 2003, *Rev. Mex. A&A. Conf.*, 15, 20
- Preite-Martinez, A. 1988, *A&AS*, 76, 317
- Ratag, M. A., Pottasch, S. R., Zijlstra, A. A., & Menzies, J. 1990, *A&A*, 233, 181
- Reid, M. J., Muhleman, D. O., Moran, J. M., Johnston, K. J., & Schwartz, P. R. 1977, *ApJ*, 214, 60
- Sahai, R., Te Lintel Hekkert, P., Morris, M., Zijlstra, A., & Likkell, L. 1999, *ApJ*, 514, L115
- Sevenster, M. N. 2002, *AJ*, 123, 2772
- Sevenster, M. N., Chapman, J. M., Habing, H. J., Killeen, N. E. B., & Lindqvist, M. 1997, *A&AS*, 124, 509
- Skrutskie, M. F., et al. 2006, *AJ*, 131, 1163
- Slysh, V. I., Dzura, A. M., Val'tts, I. E., & Gerard, E. 1997, *A&AS*, 124, 85
- Suárez, O., García-Lario, P., Manchado, A., Manteiga, M., Ulla, A., & Pottasch, S.R. 2006, *A&A*, 458, 173.
- Suárez, O., Gómez, J. F., Morata, O. 2007, *A&A*, 467, 1085.
- Tafoya, D., et al. 2007, *AJ*, 133, 364
- Thompson, D. J., et al. 1995, *ApJS*, 101, 259
- Torrelles, J. M., Patel, N. A., Gómez, J. F., & Anglada, G. 2002, *Rev. Mex. A&A Ser. Conf.*, 13, 108

Velázquez, P. F., Gómez, Y., Esquivel, A., & Raga, A. C. 2007, MNRAS, 382, 1965

Yusef-Zadeh, F., & Bally, J. 1987, Nature, 330, 455

Zijlstra, A. A., Te Lintel Hekkert, P., Pottasch, S. R., Caswell, J. L., Ratag, M., & Habing,
H. J. 1989, A&A, 217, 157

Table 1. Observational parameters: line data

Molecule	ν_o^a (MHz)	Date ^b	Conf ^c	F _{Cal} ^d	S_{FCal}^e (Jy)	P _{Cal} ^f	S_{PCal}^e (Jy)	BW ^g (MHz)	N_c^h	ΔV^i (km s ⁻¹)
H ₂ O	22235.08	2006-JAN-02	D	J1331+305	2.54	J1820-254	0.744 ± 0.017	3.125	64	0.66
H ₂ O	22235.08	2006-OCT-06	CnB	J1331+305	2.54	J1820-254	0.682 ± 0.022	3.125	64	0.66
OH	1612.2310	2006-OCT-15	CnB	J1331+305	13.85	J1751-253	0.921 ± 0.017	1.5625	256	1.14
OH	1665.4018	2006-NOV-22	C	J1331+305	13.63	J1751-253	1.049 ± 0.007	1.5625	128	2.20

^aRest frequency of the transition.

^bDate of observation. On 2006-JAN-02, only IRAS 18061–2505 was observed. On 2006-OCT-06, IRAS 17443–2949 and IRAS 17580–3111 were observed. On the other two dates, all three sources were observed.

^cConfiguration of the VLA.

^dFlux and bandpass calibrator

^eFlux density of calibrators.

^fPhase calibrator.

^gBandwidth.

^hNumber of observed spectral channels.

ⁱVelocity resolution.

Table 2. Observational parameters: continuum data

$\nu_{\text{sky}}^{\text{a}}$ (MHz)	Date ^b	Conf ^c	FCal ^d	$S_{\text{FCal}}^{\text{e}}$ (Jy)	PCal ^f	$S_{\text{PCal}}^{\text{e}}$ (Jy)	BW ^g (MHz)
22283	2006-JAN-02	D	J1331+305	2.54	J1820-254	0.729 ± 0.016	25
22283	2006-OCT-06	CnB	J1331+305	2.54	J1820-254	0.688 ± 0.016	25
1685	2006-NOV-22 ^h	C	J1331+305	13.55	J1751-253	1.18 ± 0.04	25

^aCentral sky frequency of the observation.

^bDate of observation. On 2006-JAN-02, only IRAS 18061–2505 was observed. On 2006-OCT-06, IRAS 17443–2949 and IRAS 17580–3111 were observed. On 2006-NOV-22, all three sources were observed.

^cConfiguration of the VLA.

^dFlux and bandpass calibrator.

^eFlux density of calibrators.

^fPhase calibrator.

^gBandwidth.

^hThese data were not usable, due to radio frequency interference.

Table 3. Parameters of target sources and maps

IRAS name	Obs type ^a	R.A.(J2000) ^b	Dec(J2000) ^b	$V_{\text{LSR}}^{\text{c}}$ (km s^{-1})	$\theta_{\text{syn}}^{\text{d}}$ (arcsec)	p.a. ^e (degree)
17443–2949	OH-1612	17 47 35.30	–29 50 57.0	–5.0	13.0×8.0	–78
	OH-1665	17 47 35.30	–29 50 57.0	–5.0	29.2×9.0	–7
	H ₂ O+cont	17 47 35.30	–29 50 54.2	–5.0	0.78×0.70	72
17580–3111	OH-1612	18 01 19.60	–31 11 22.0	22.0	12.4×8.3	80
	OH-1665	18 01 19.60	–31 11 22.0	22.0	30.0×9.0	2
	H ₂ O+cont	18 01 19.70	–31 11 23.0	22.0	1.1×0.5	44
18061–2505	OH-1612	18 09 12.40	–25 04 34.0	60.0	14.0×5.7	65
	OH-1665	18 09 12.40	–25 04 34.0	60.0	25.8×9.4	13
	H ₂ O+cont	18 09 12.40	–25 04 34.0	60.0	5.3×2.6	–7

^aType of observation. OH-1612: OH maser line, rest frequency 1612 MHz; OH-1665: OH maser line, rest frequency 1665 MHz; H₂O+cont : Water maser line and continuum, simultaneous observations at 22 GHz.

^bCoordinates of the phase center of the observations. Units of right ascension are hours, minutes, and seconds. Units of declination are degrees, arcminutes, and arcseconds.

^cVelocity of the bandwidth center with respect to the Local Standard of Rest (LSR), for line observations.

^dFull width at half maximum of the synthesized beam of the map.

^ePosition angle (north to east) of the major axis of the synthesized beam.

Table 4. Detected maser components and upper limits of non-detections

IRAS	line	R.A.(J2000)	Dec(J2000)	Δp^a (milliarcsec)	V_{peak}^b (km s ⁻¹)	S_{peak}^c (Jy)
17442–2942	OH-1612	17 47 28.867	–29 43 37.98	300 × 170	–55.9	0.229
		17 47 28.896	–29 43 38.41	400 × 250	–24.1	0.158
	OH-1665	≤ 0.010
17443–2949	OH-1612	17 47 35.22	–29 50 53.5	900 × 600	–4.8	0.056
		17 47 35.442	–29 50 53.32	40 × 30	–16.1	1.215
	OH-1665	17 47 35.16	–29 50 57.6	4000 × 1200	2.6	0.023
		17 47 35.27	–29 50 52.0	3000 × 800	–10.6	0.032
		17 47 35.32	–29 50 54.1	1400 × 400	–6.2	0.063
	H ₂ O ^d	17 47 35.326	–29 50 53.05	600 × 190	–15.0	0.141
		17 47 35.3253	–29 50 53.369	6 × 5	0.9	0.690
		17 47 35.32871	–29 50 53.3563	0.8 × 0.7	–3.7	5.683
17 47 35.33063		–29 50 53.3984	0.6 × 0.5	–6.3	6.912	
17579–3121	OH-1612 ^d	17 47 35.331	–29 50 53.34	50 × 40	–1.7	0.079
		18 01 13.3709	–31 21 56.596	10 × 7	21.8	4.504
		18 01 13.3771	–31 21 57.000	13 × 9	1.4	2.100
		18 01 13.399	–31 21 57.38	190 × 130	33.2	0.134
	OH-1665	≤ 0.010
17580–3111	OH-1612 ^d	18 01 20.3987	–31 11 20.548	15 × 10	28.6	1.604
		18 01 20.3992	–31 11 20.582	30 × 21	12.7	0.912
	OH-1665	≤ 0.008
	H ₂ O	18 01 20.3923	–31 11 21.305	21 × 11	17.4	0.418
18061–2505	OH-1612	≤ 0.011

Table 4—Continued

IRAS	line	R.A.(J2000)	Dec(J2000)	Δp^a (milliarcsec)	V_{peak}^b (km s ⁻¹)	S_{peak}^c (Jy)
	OH-1665	≤ 0.007
	H ₂ O ^d	18 09 12.4022	-25 04 34.396	4×1.8	57.4	1.384
		18 09 12.4032	-25 04 34.431	1.0×0.5	60.7	5.682
		18 09 12.4033	-25 04 34.417	10×5	63.9	0.693

^aRelative positional uncertainties within maps for each maser transition and source. Quoted uncertainties are 2σ errors, and have been estimated as $\Delta p = \theta_{\text{syn}} \frac{\sigma_{\text{map}}}{S_{\text{peak}}}$, where θ_{syn} is the synthesized beam, and σ_{map} is the rms noise level of the map. The position angle of the error ellipse is the same as that of the synthesized beam. Absolute astrometric errors can be estimated by quadratically adding these values to the intensity-independent uncertainties, roughly one tenth of the synthesized beam of each map.

^bSR velocity of the peak of each individual spectral component. Its uncertainty is determined by the velocity resolution of the data.

^cPeak flux density of individual spectral components, or upper limits for non-detections. Typical 2σ errors are 5-10 mJy. Upper limits are 3σ . Values have not been corrected by primary beam response.

^dData were Hanning-smoothed in frequency. The resulting spectral resolution is double of their corresponding value in Table. 1.

Table 5. Continuum emission

IRAS	ν_{sky} (MHz)	R.A.(J2000)	Dec(J2000)	S_ν (mJy)
17442–2941	1665	≤ 0.9
17443–2949	1665	≤ 0.9
	22284	≤ 1.0
17579–3121	1665	≤ 0.5
17580–3111	1665	≤ 0.5
	22282	≤ 1.4
18061–2505	1665	18 09 12.563	–25 04 32.51	2.6 ± 0.9
	22283	18 09 12.4036	–25 04 34.383	38.1 ± 0.6

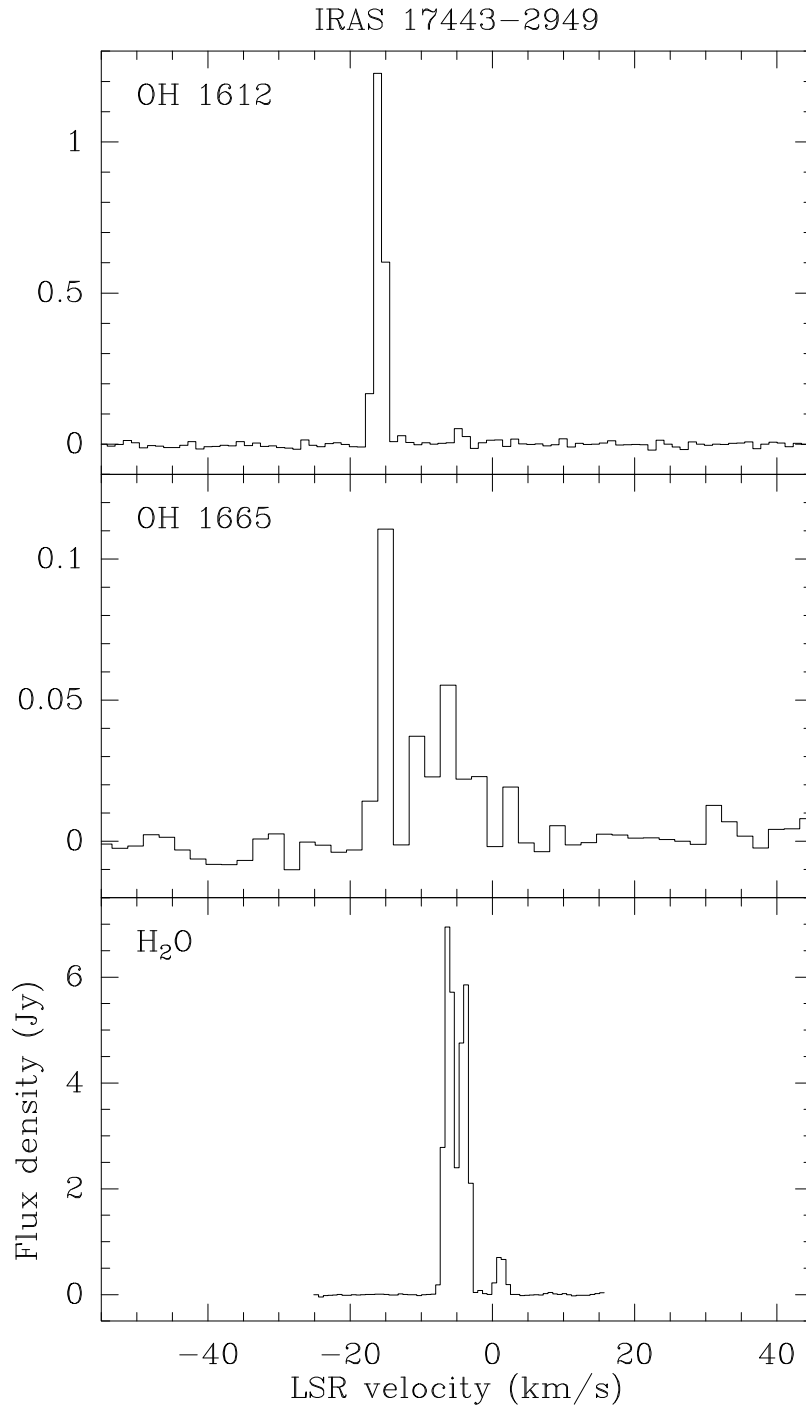


Fig. 1.— OH and H₂O maser spectra toward IRAS 17443-2949

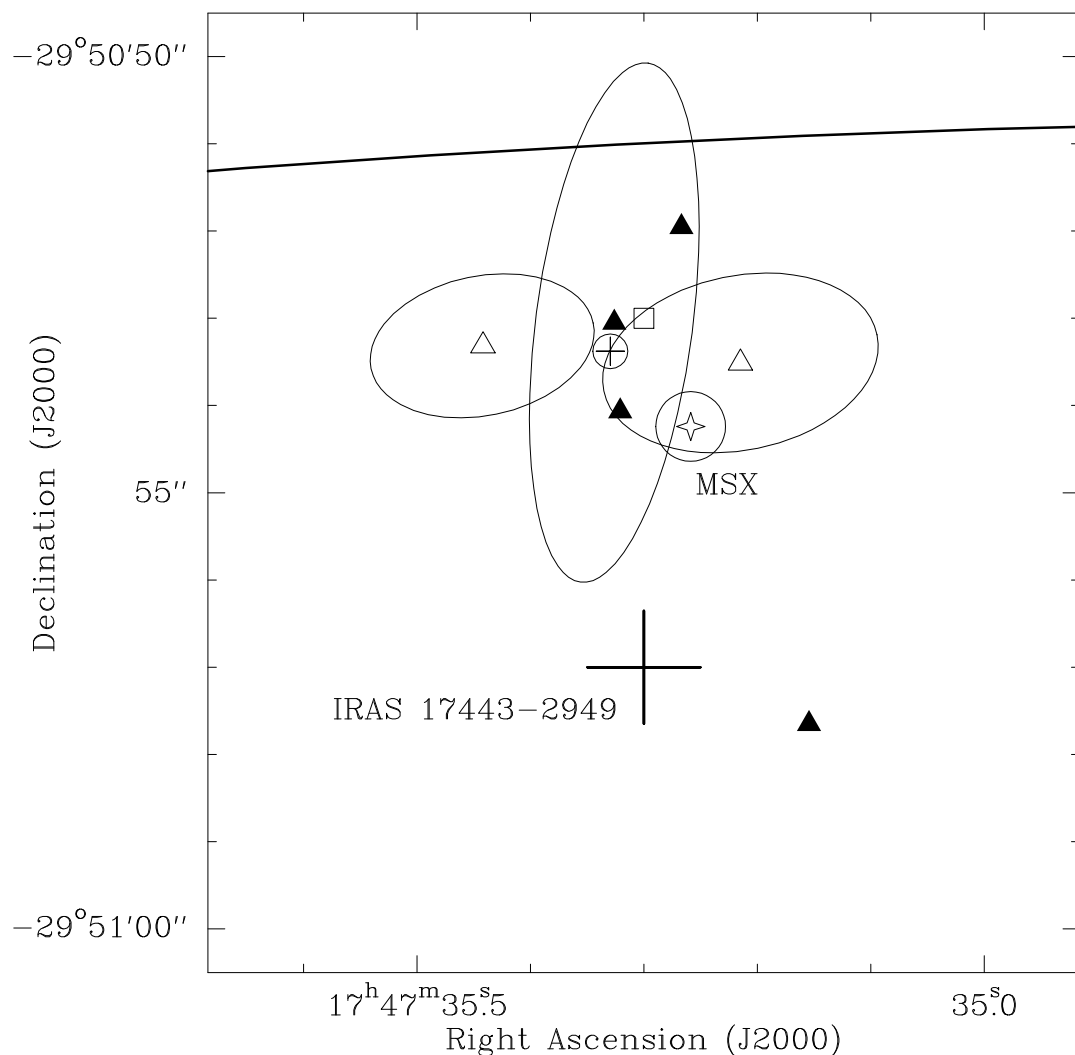


Fig. 2.— Positions of maser components and infrared sources in the IRAS 17443–2949 region. Open and filled triangles represent the OH maser components at 1612 MHz and 1665 MHz, respectively. The small cross represents the mean position of the H₂O maser components. The large cross marks the position of IRAS 17443–2949 in the IRAS point source catalog. The four-pointed star is the position of the MSX infrared source MSX6C G359.4428-00.8398. Ellipses represent the estimated absolute positional error of each source and maser component (for OH-1665-MHz only the error ellipse of the component with best positional accuracy is plotted). The thick curve is part of the error ellipse of the IRAS source position (semiaxes of the error ellipse: 34'' × 6'', p.a. = 93°). The open square is the position of the 1612-MHz OH maser reported by Zijlstra et al. (1989), for which we did not plot an error ellipse.

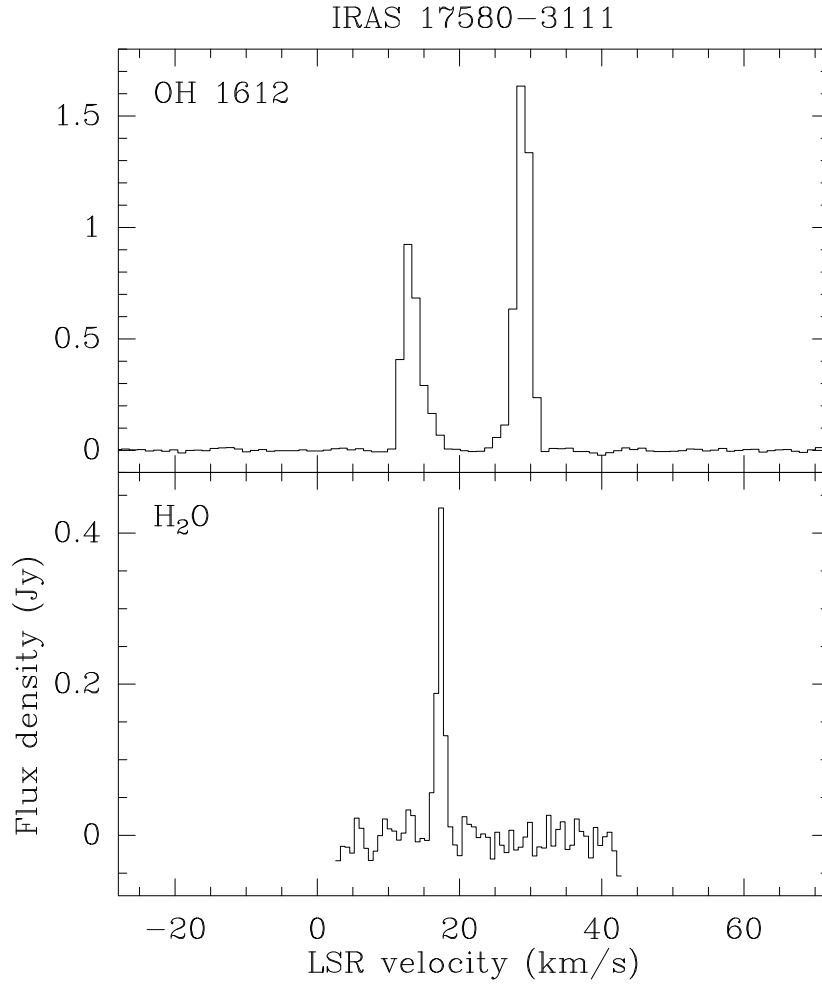


Fig. 3.— OH and H₂O maser spectra toward IRAS 17580-3111.

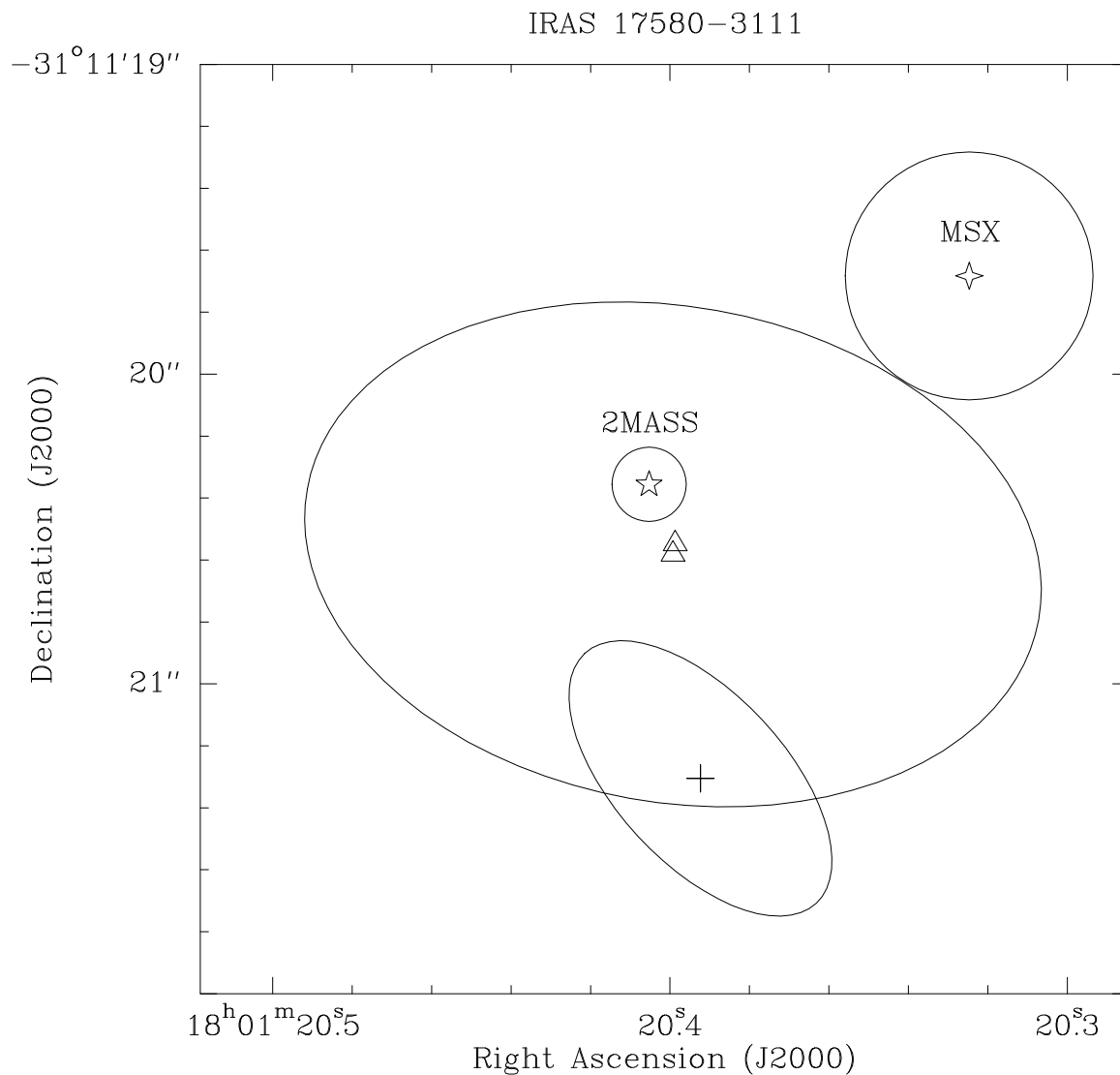


Fig. 4.— Positions of maser components and infrared sources in the IRAS 17580–3111 region. The cross and open triangle represent the H₂O and OH-1612-MHz maser components, respectively. The four-pointed star is the position of the MSX infrared source MSX6C G359.7798-04.0728. The five-pointed star marks the position of the source 2MASS J18012040-3111203. Ellipses represent the estimated absolute positional error of each component and source. The whole area shown is within the error ellipse of IRAS 17580–3111 [located at R.A.(2000) = 18^h01^m19.6^s, Dec.(2000) = –31°11′20″. Error ellipse semiaxes: 38″ × 7″, p.a. = 91°].

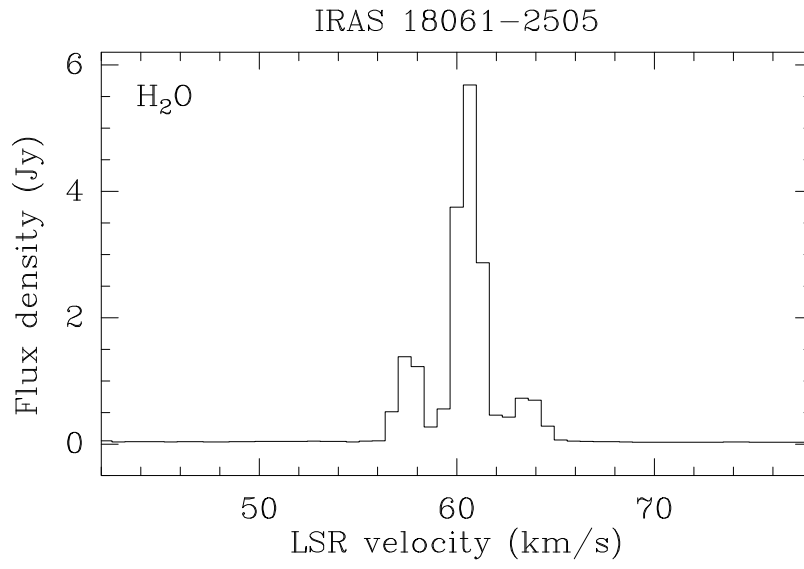


Fig. 5.— H₂O maser spectrum toward IRAS 18061–2505.

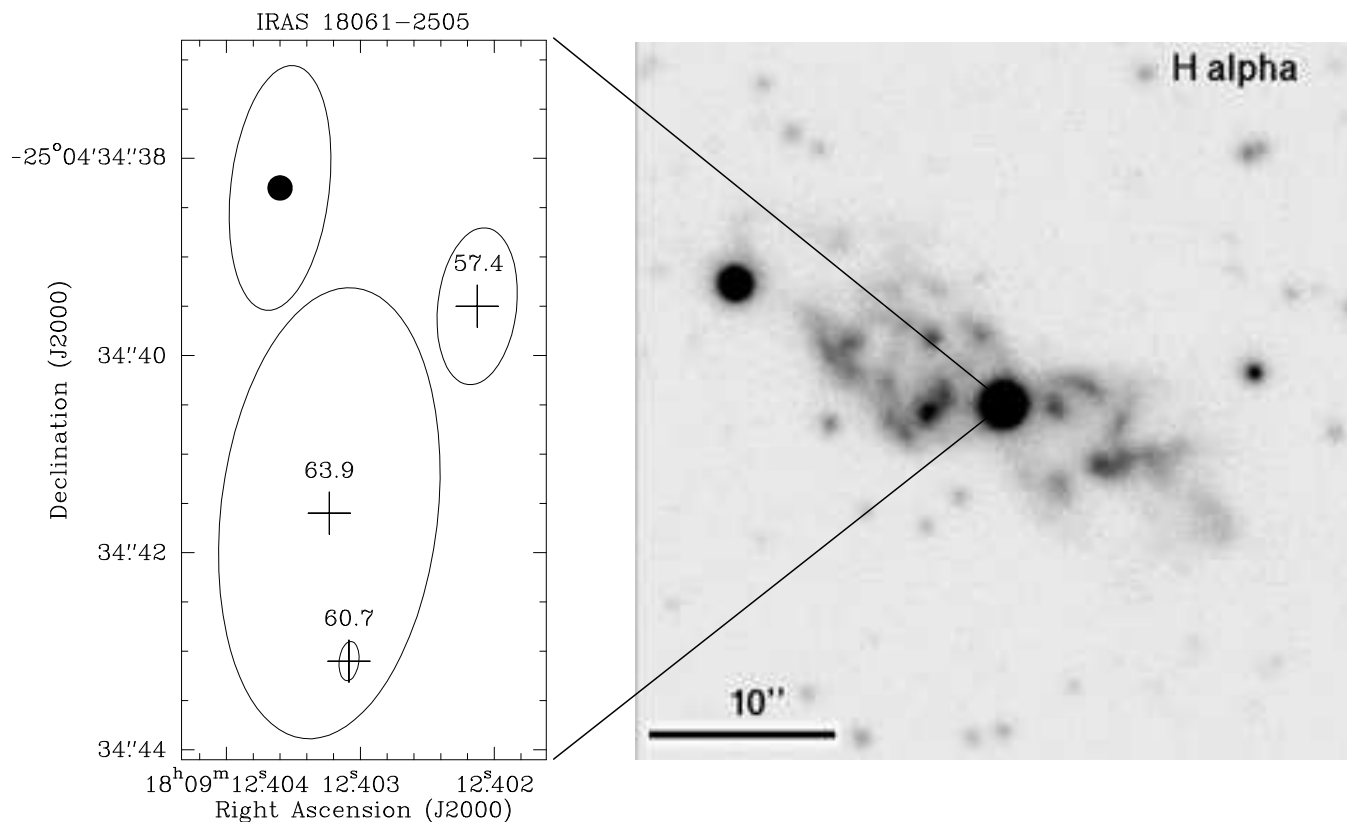


Fig. 6.— Left: Positions of H_2O maser components (crosses) and 1.3 cm radio continuum emission (filled circle) in the IRAS 18061–2505 region. Ellipses represent the *relative* positional errors within the map. Absolute positional errors are $\simeq 0''.5$. The H_2O components are labelled with their LSR velocities, in km s^{-1} . Right: H_α image from Suárez et al. (2006). Note the very different spatial scales in both images.

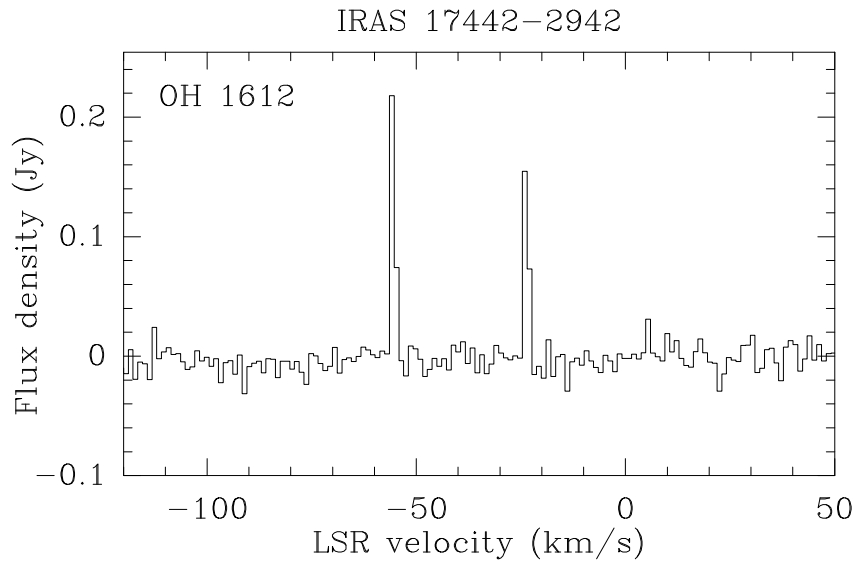


Fig. 7.— OH maser spectrum toward IRAS 17442-2942.

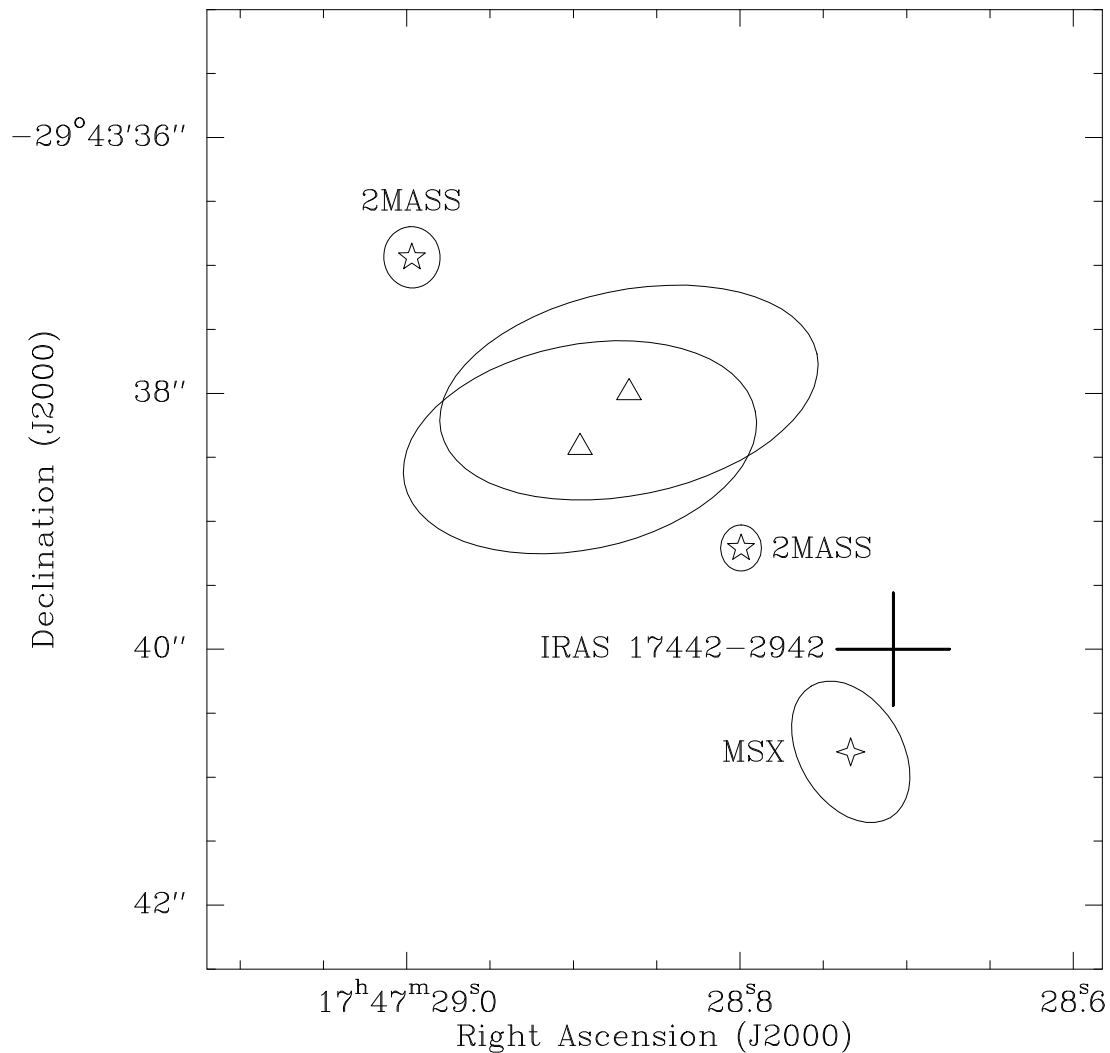


Fig. 8.— Positions of maser components in and infrared sources in the IRAS 17442–2942 region. The open triangles mark the location of the OH maser components at 1612 MHz. The cross marks the position of IRAS 17442–2942 in the IRAS point source catalog (semiaxes of error ellipse: $50'' \times 7''$, p.a. = 92°). The four-pointed star is the position of the MSX infrared source MSX6C G359.5336-00.7573. The five-pointed stars mark the position, in order of increasing right ascension, of sources 2MASS J17472879-2943392 and 2MASS J17472898-2943369. Solid ellipses represent the estimated absolute positional error of each component and source.

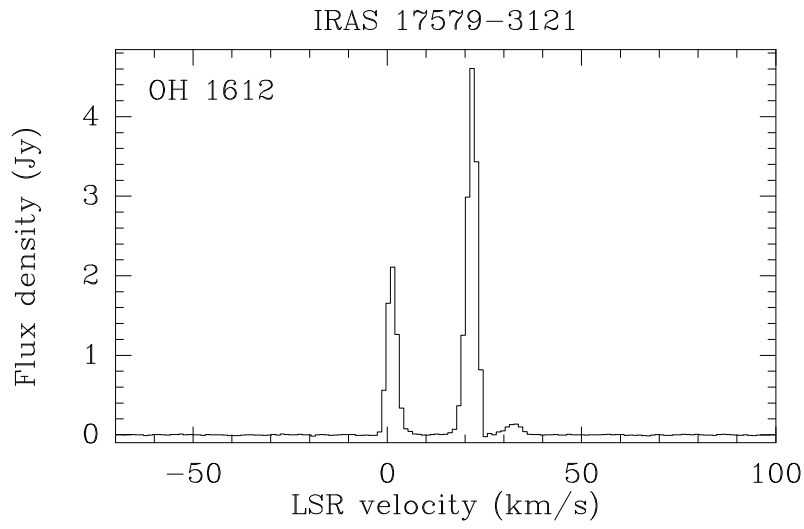


Fig. 9.— OH maser spectrum toward IRAS 17579–3121.

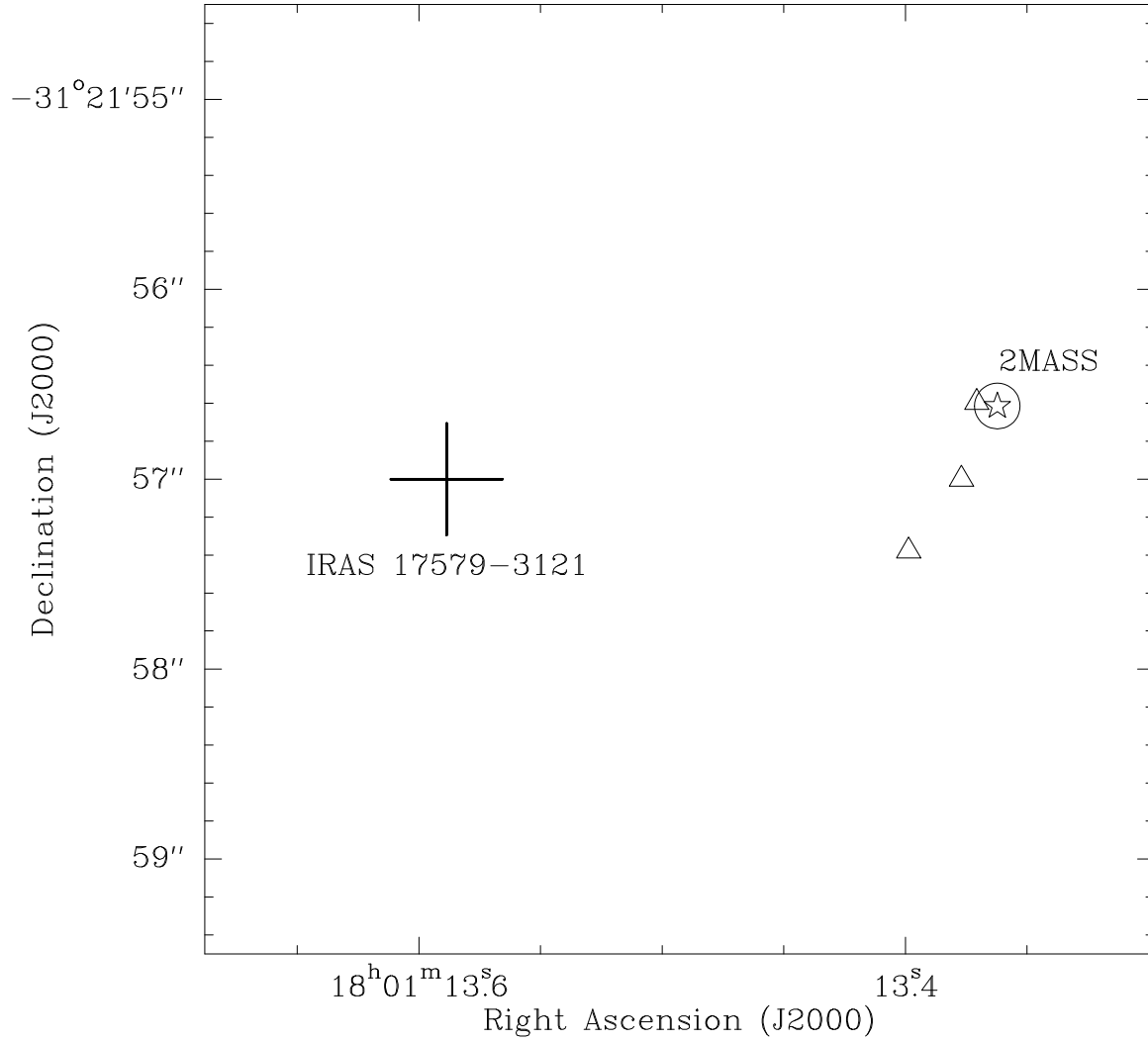


Fig. 10.— Position of OH maser components and infrared sources in the IRAS 17579–3121 field. Open triangles represent the OH masers at 1612 MHz. The five-pointed star marks the position of 2MASS J18011337-3121566. Absolute position errors of OH maser components are $\simeq 1''$. The large cross marks the position of the IRAS source (semiaxes of the error ellipse are $39'' \times 8''$, p.a. = 91°)